Journal of Colloid and Interface Science 497 (2017) 378–384

Contents lists available at ScienceDirect

Journal of Colloid and Interface Science

journal homepage: www.elsevier.com/locate/jcis

A hybrid molecular dynamics study on the non-Newtonian rheological behaviors of shear thickening fluid

Kaihui Chen, Yu Wang *, Shouhu Xuan, Xinglong Gong *

CAS Key Laboratory of Mechanical Behavior and Design of Materials, Department of Modern Mechanics, University of Science and Technology of China (USTC), Hefei 230027, PR China

GRAPHICAL ABSTRACT

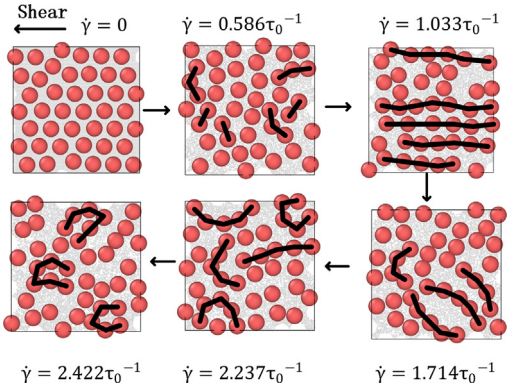

ARTICLE INFO

Article history:
Received 23 December 2016
Revised 6 March 2017
Accepted 6 March 2017
Available online 8 March 2017

Keywords:
Shear thickening
Microstructure
Molecular dynamics
Stochastic rotation dynamics

ABSTRACT

To investigate the microstructural evolution dependency on the apparent viscosity in shear-thickening fluids (STFs), a hybrid mesoscale model combined with stochastic rotation dynamics (SRD) and molecular dynamics (MD) is used. Muller-Plathe reverse perturbation method is adopted to analyze the viscosities of STFs in a two-dimensional model. The characteristic of microstructural evolution of the colloidal suspensions under different shear rate is studied. The effect of diameter of colloidal particles and the phase volume fraction on the shear thickening behavior is investigated. Under low shear rate, the two-atom structure is formed, because of the strong particle attractions in adjacent layers. At higher shear rate, the synergetic pair structure extends to layered structure along flow direction because of the increasing hydrodynamics action. As the shear rate rises continuously, the layered structure rotates and collides with other particles, then turned to be individual particles under extension or curve string structure under compression. Finally, at the highest shear rate, the strings curve more severely and get into two-dimensional cluster. The apparent viscosity of the system changes from shear-thinning behavior to the shear-thickening behavior. This work presents valuable information for further understanding the shear thickening mechanism.

1. Introduction

In recent year, shear thickening fluid (STF) as an added material on body armor has gained substantial attention for impact absorbers. After its impregnation into the fabric, the thickness and stiff-

* Corresponding authors.
E-mail addresses: wyu@ustc.edu.cn (Y. Wang), gongxl@ustc.edu.cn (X. Gong).

http://dx.doi.org/10.1016/j.jcis.2017.03.038
0021-9797/

ness of the fabric show little change while the phenomenon of shear thickening (ST), which is inherent to STF, significantly enhances the ballistic resistance. ST phenomenon is one remarkable non-Newtonian rheological behavior in STF, which induces dramatic change in suspension microstructure. As a result, the viscosity will increase potentially by orders of magnitude beyond a certain shear rate. This behavior is reversible so the stress relaxes when the external shear load is removed. ST phenomenon is widely found in dense packed colloids or suspensions, which is also a concern across a range of other industrial processes involving lubricating oils, foods, powder conveying, polishing and even within the human body [1–7]. All the applications require a fundamental understanding of the complex rheological behavior of the suspension and underlying microstructure evolution during the shear flow.

The mechanism of ST behavior in colloidal suspensions has been discussed in some literatures. Hoffman [8] used light diffraction combined with shear rheology to investigate microstructural details during the ST process. He proposed an order-disorder transition, in which the flow structure changes from an ordered structure to a disordered structure, which also results in an increase in drag forces between particles. Dratler et al. [9] also thought that there was a similar transition in suspensions microstructure at the onset of ST phenomenon. However, other researchers [10–13] confirmed that under some conditions, the ST behavior could occur without order-to-disorder transition through simulation and experiments. Up to now, the most acceptable approach is the formation of "hydro-cluster" in suspensions [14–23], which is responsible for the continuous viscosity increase during the shear process and which has been observed for Brownian suspensions with moderate volume fractions. From the research results [10–23], it can be concluded that suspended particles would flow freely and get into equilibrium state at low shear-rate, then get gathered together and turn into dynamic equilibrium under higher shear rates. And yet, the link between the microstructure evolution of hydro-clusters and continuous shear thickening (CST) for non-Brownian suspensions is still a matter of debate [21]. Moreover, in contrast to a continuous viscosity increase at any applied shear rate, the discontinuous shear thickening (DST) is observed when the volume fraction of the flowing suspension is increased above a critical value. Some researchers [22–24] confirmed that the jamming of suspensions took responsible for the DST. Peter et al. [22] considered DST an independent phenomenon from shear-jammed transitions and jamming states, and they confirmed DST the conclusion of frictional contacts between particles.

Besides the discussion of the origins of ST, researchers also concerned about the influence factors on this special nonlinear behavior, such as phase volume fraction, particle size, etc. [14,25–31]. Brown et al. [30] found that increasing the packing fraction of cornstarch in water would eliminate the occurrence of ST phenomenon. Zhang et al. [31] used small fume silica (14 nm) and large particle of silica (1–5 μm) to fabricate the STF with ethylene glycol. It was found that the 14 nm silica had significant ST effect, unlike the large particle in the suspension. The DST behavior was also found dependent on the system properties, e.g., particle dispersibility or shape, as well as the flow geometry [27,28]. Even though many researchers [32–35] have demonstrated that the viscosity is firmly associated with the microstructure of colloidal particles in many solutions, there is still no direct observations of the evolution law under different influence factor of STFs and the influence mechanism of STFs is still unclear. Although many researchers have explored the STFs through Stokesian Dynamics [36], dissipative particle dynamics [37], and dynamic discrete element method [38], the evolution of microstructure of colloidal particles with ST phenomenon is still in a lack of direct observations to prove the microscopic mechanisms of STF. Therefore, a systematic investigation on this issue should be performed. Our work concerns on the relationships of transitions of microstructure and the viscosity under different shear rate in STF, so as to study the mechanism for ST phenomenon via numerical simulations.

In this work, the non-Newtonian rheological behavior of STF is studied by a hybrid model combining the molecular dynamics (MD) method and stochastic rotation dynamics (SRD) method. In the next section, we briefly review the basics of the hybrid model and the implementation of the Muller-Plathe (MP) reverse perturbation method for colloidal suspensions. The computation details are introduced at the end of this section. In Section 3, the non-Newton rheological behavior is studied. The relationship between the microstructural evolution and the ST behavior is analyzed. And then the influence factor on the ST behavior is discussed. Finally, the conclusion of the simulation results is drawn in the last section.

2. Simulation technique

2.1. The hybrid SRD-MD mesoscopic model

The fundamental principles of the method used here have been explained extensively elsewhere [39,40], and therefore only the most important parts will be described here. In this work, the colloidal particles are modeled with MD algorithm, while the solvent particles are simulated with SRD method. The first part of the method is the SRD method. SRD, also known as multi-particle collision dynamics (MPC), is a particle-based mesoscale simulation method for complex fluids which fully incorporates thermal fluctuations and hydrodynamic interactions. It can be seen as a "hydrodynamic heat bath". In SRD, the solvent is modeled by a large number N of point-like particles. The multi-particle system is divided into cubic cells of regular lattices with no restriction on the number of particles in a cell. The evolution of the system consists of two steps: streaming and collision. In the streaming step, the coordinate of each particle is incremented by its displacement during the time step. Collisions are modeled by a simultaneous stochastic rotation of the relative velocities of every particle in each cell. The procedure is briefly described as followed:

Consider a set of N point particles with (continuous) coordinates $r_i(t)$ and velocities $v_i(t)$. During the streaming step, the ith SRD particle's position at time n + 1 is calculated via the simple forward Euler scheme:

$$\mathrm{r}_\mathrm{i}^{\mathrm{n}+1} = \mathrm{r}_\mathrm{i}^{\mathrm{n}} + \mathrm{v}_\mathrm{i}^{\mathrm{n}}\Delta\mathrm{t}, \tag{1}$$

Δt is the value of the simulation timestep. For the collision step, particles are sorted into cells, and they interact only with the particles in their own cells. Then an independent random rotation of the relative velocities $\boldsymbol{v_i} - \boldsymbol{u}$ will be applied to the particles in each cell, where the macroscopic velocity $\mathrm{u}(\xi, t)$ is the mean velocity of the particles in the cell with coordinate ξ. The local temperature $\mathrm{T}(\xi,t)$ is defined via the mean square deviation of the particle velocities from the mean velocity in a cell. The rotation angles of different cells are statistically independent. Throughout the process, the local momentum and kinetic energy are invariant. The velocity of ith particle at time step (n + 1) during the collision step is updated from that at time step n by:

$$\mathrm{v}_\mathrm{i}^{\mathrm{n}+1} = \mathrm{v}_\mathrm{i}^{\mathrm{n}} + \mathrm{R}[\xi(\mathrm{r}_\mathrm{i}^{\mathrm{n}+1})]\{\mathrm{v}_\mathrm{i}^{\mathrm{n}} - \mathrm{u}[\xi(\mathrm{r}_\mathrm{i}^{\mathrm{n}+1})]\}, \tag{2}$$

where $\mathrm{R}[\xi(r_i^{n+1})]$ denotes a stochastic rotation matrix. R is taken to be a rotation by an angle ±α, with probability 1/2. The value of α is set to be 90°. In every time step for each cell, one of these 6 possibilities is chosen with equal probability 1/3.

The second part of the hybrid mesoscopic method is description of dynamic behavior of the colloidal particles under the interaction

between particles. An MD simulation of the colloidal particle is coupled to an SRD simulation of the fluid, by numerically integrating Newton's equation of motion for the colloidal particle using the velocity-Verlet algorithm [41] between collisions with a smaller time step $\Delta t_{MD} < \Delta t_{SRD}$. The colloidal particle interacts with the solvent particle in the collision step of SRD algorithm. In this step, the solvent particles and any colloidal particles in the same cell exchange momentum through the same collision rule as the pure solvent particles described above. The inter-particle force in the solvent particles system is based on the 12-6 Lennard-Jones (L-J) potential, which is given by:

$$U_{LJ}(r) = \begin{cases} 4\varepsilon\left[\left(\frac{\sigma}{r}\right)^{12} - \left(\frac{\sigma}{r}\right)^{6}\right] & for\ r < r_c \\ 0 & for\ r \geqslant r_c \end{cases}, \quad (3)$$

where σ is the finite distance at which the inter-particle potential is zero, ε is the depth of the potential well, and r is the center-to-center distance between the particles. ε_0 and σ_0 are the units of energy and distance. And the colloidal-solvent distance σ_{cs} is set to be half of colloidal-colloidal distance σ_{cc} to reduce false energy dissipation. For colloidal particles, the mass is defined as m_0, and the mass of solvent particles is set as 0.01 m_0. The temperature of the simulation system is set as $T_0 = 1.0\varepsilon_0/K_B$, where K_B is Boltzmann's constant. In our simulation, the standard of time is defined as $\tau_0 = (\sigma_0^2 m_0/\varepsilon_0)^{1/2}$, and the time step of MD is set as $\Delta t_{MD} = 0.001\tau_0$, while the timestep of SRD part is set as $\Delta t_{SRD} = 20\Delta t_{MD} = 0.02\tau_0$. Here the cut-off radius of interactions of colloidal particles is set as $r_c = 5\sigma_0$. All parameters used in our simulation are in L-J units.

2.2. MP reverse perturbation method

The MP reverse perturbation method [42,43] is used in this paper. The momentum flux is imposed on the system as follows: The periodic simulation box is subdivided into n slaps along the z coordinate, where n is an even number. The slabs from top to bottom are marked as 1, 2, …, n. The atoms inside the slab 1 (and its period images) are propelled in the −x direction, and those inside the slab (n/2 + 1) move in the +x direction. Two particles are then identified, one in the 1st slab and the other in the (n/2 + 1)th slab, such that their velocities, v_x, are opposed to the desired streaming direction of the corresponding slab. Then, the momentum, Δp_x, is exchanged between the two particles. The entire process is repeated at a set interval to produce the desired shear rate. The total momentum transferred in a simulation P_x is the sum of the Δp_x. The system responds to the nonequilibrium situation by letting momentum flow in the opposite direction via a physical mechanism (friction). In the steady state, the rate of momentum transferred by momentum swaps is equal to that of momentum flowing back through the fluid by friction. According to the total momentum transfer, the momentum flux $j_z(p_x)$ can be calculated:

$$j_z(p_x) = \frac{P_x}{2tA} \quad (4)$$

where t is the length of the simulation and $A = L_x L_y$,the factor 2 arises because of the periodicity of the system. And the induced velocity profile is composed of two approximately linear profiles mirrored about the middle of the first and middle slab. This velocity profile, $(\partial v_x/\partial z)$, can be related to the imposed momentum transfer and fluid viscosity:

$$j_z(p_x) = -\eta\frac{\partial v_x}{\partial z}, \quad (5)$$

In other simulations [13,36–38,44–49], the shear deformation is introduced either by using Lees-Edwards boundary conditions or by setting the mean velocity u in the cells at the border to the shear velocity. Different from the nonequilibrium MD simulations, the MP reverse perturbation method imposed the momentum through a series of momentum exchanges between particles within the system. And the total momentum and total energy are conserved in the MP procedure. If the momentum transfer in the procedure and the final shear velocity profile of the entire system can be determined, it is simple to obtain the viscosity of the system as shown in Eq. (5).

2.3. Computational model details

According to the results of Xiang Cheng et al. [50,51], the microstructure evolution of the colloidal suspension mainly occurs in the gradient plane under shear. In addition, we also set up the three-dimensional model and two-dimensional model with the same particle size and phase volume ratio to confirm the consistency of the microstructure evolution. It is found that the ST behavior and the main features of microstructure evolution are similar in both models. Therefore, here the two-dimensional model is adopted in the simulation. Firstly, the colloidal particles are uniformly arranged in the simulation box, and the solvent particles are then added in this box. The overlap solvent particles are detected to ensure the whole initial system in the reasonable physical configuration. Then 2×10^6 steps of equilibrium run are taken to make all particles distributing uniformly. Finally, 5×10^6 steps with application of certain shear rate on particles are taken to calculate viscosities. The two-dimensional simulation box is at size of L_x = 11.66 σ_0 and L_z = 11.66 σ_0. The diameters of colloidal particles and the volume fractions of the colloidal particles are varied for determining the influencing rule on the ST behavior. Considering Refs. [36–38,52] and experiments, particle diameter σ_0 is chosen to be 440 nm, colloidal particle density is 1.9×10^3 kg/m^3, particle mass m_0 is set as 8.5×10^{-17} kg, and simulation temperature T_0 is considered as 293 K. The values of parameters used here are consistent with the literature [52] in order of magnitude.

3. Results and discussions

3.1. Typical shear-thickening behavior in suspension solutions

The non-Newtonian rheological behavior of a typical suspension system is analyzed by hybrid SRD-MD methods. The diameter of the colloidal particle is $1.52\sigma_0$, the potential well depth of the L-J potential is $1.52\varepsilon_0$, the corresponding distance of the zero potential is $1.52\sigma_0$ and the volume fraction of the colloidal particles in the whole solution system is 58%. As shown in Fig. 1(a), the results clearly show that such a solution system exhibits a typical CST behavior. The shear viscosity is $3.748\varepsilon_0\tau_0/\sigma_0^3$ at shear rate of $0.586\tau_0^{-1}$. As the shear rate increases, the viscosity decreases first and then reaches the minimum value of $3.541\varepsilon_0\tau_0/\sigma_0^3$ at the shear rate of $1.033\tau_0^{-1}$. Increasing the shear rate from this point, the viscosity increases continuously. Fig. 1(b) shows the average velocity of the layers under different shear rates. As we can see, the velocity of each shear rate is symmetrical about the middle layer, the 11th layer. The velocity profiles on each half side are nearly linear, though there is a small disturbance under low shear rate.

As shown in the schematic illustration in Fig. 2, the simple shear can be resolved into pure rotation and pure shear strain. In addition to the rotational movement, the atoms in system will be compressed or extended along the ±45° direction. From the initial equilibrium configuration (Fig. 3-a), the particles of the whole system are distributed uniformly and all particles are spaced apart from each other. At low shear rate (Fig. 3-b), the hydrodynamic contribution of the system is weak, and the Brownian motion is dominated. Due to the mutual attraction between the particles,

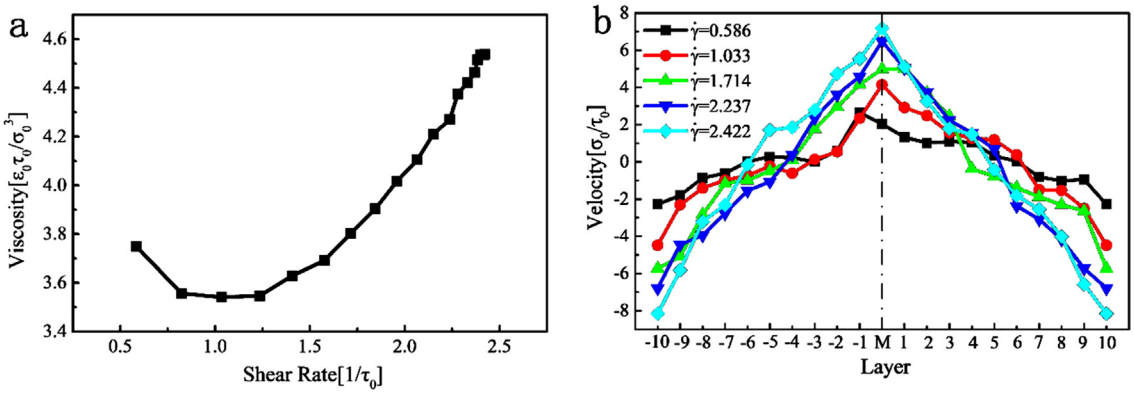

Fig. 1. (a) The shear viscosity versus shear rate for the Non-Newtonian suspension fluid, of which the volume fraction is 58%, the mass fraction is 70%, the colloidal particle diameter is $1.52\sigma_0$, the potential well depth of the L-J potential is $1.52\varepsilon_0$ and the corresponding distance of the zero potential is $1.52\sigma_0$. (b) The velocity profiles of each layer at shear rate of $0.586\tau_0^{-1}$, $1.033\tau_0^{-1}$, $1.714\tau_0^{-1}$, $2.237\tau_0^{-1}$, $2.422\tau_0^{-1}$.

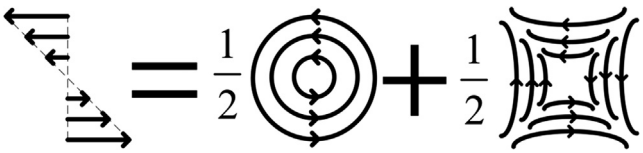

Fig. 2. The schematic illustration of simple shear.

the sliding movement of the particles in adjacent layers is lagged and the local flow resistance increases. Some small synergistic pairs of atoms are shown in the flow field (Fig. 3-b). This local synergistic pair only exists in two or three adjacent layers. And if the atoms in the pair move along the compression direction in the pure shear strain, the pair will persist for a while until the direction is changed by the rotational movement. The pair along the extension direction is visible only in a flash, and then the atoms are split with each other. With the increasing of shear rate, the hydrodynamics action enhances and the atoms in adjacent atomic layers are more compact due to the compression effect. More particles get into the synergistic atomic pairs and extend to form several orderly layered structures align the shear direction. (Fig. 3-c). And at higher shear rates (Fig. 3-d), the layered structure is unstable. The layered structure rotates and the particles in adjacent layers collide with each other and form strings of particles. The orientation of the string is random and some of them are often curved. Same as Cheng's report [50,51], such string structure is in dynamic equilibrium state, in which the particles in the chain are incorporated into or separated from the outflow by shearing action. As the shear rate further increases, the string structure curves more severely and the two-dimensional clusters appear in the flow field, as shown in Fig. 3-e. At the highest shear rate (Fig. 3-f), the two-dimensional clusters occupy the flow field as the major microstructure.

In general, the layered structure is aligned with the shear direction, which exerts smaller drag force to the local flow than the synergistic pair and the curve string. It results in the lowest apparent viscosity throughout the simulation process of the colloidal suspension system. And in the "layered structure" region, the apparent viscosity of the system changes from shear-thinning behavior

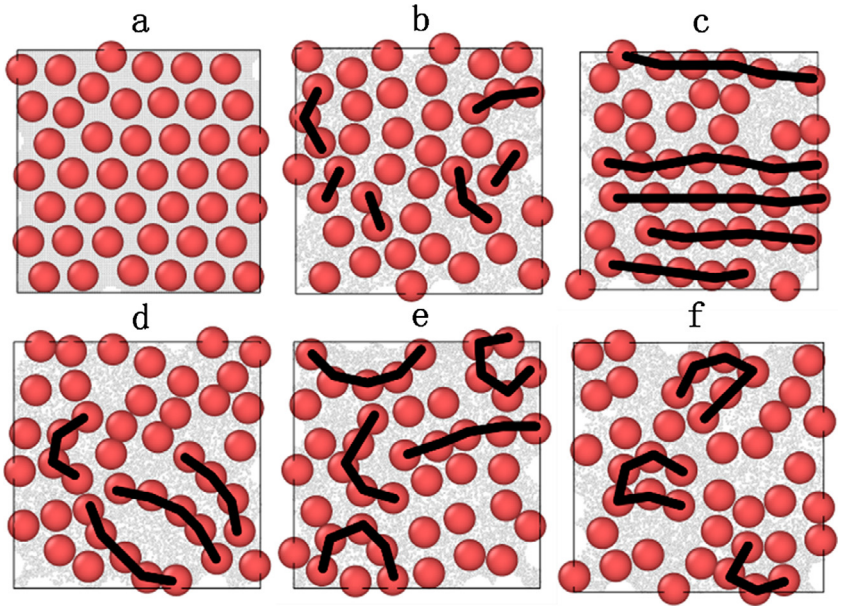

Fig. 3. The snapshots of colloidal and solvent particles with different shear rate. (a) At zero shear rate; (b) at shear rate of $0.586\tau_0^{-1}$; (c) at shear rate of $1.033\tau_0^{-1}$; (d) at shear rate of $1.714\tau_0^{-1}$; (e) at shear rate of $2.237\tau_0^{-1}$; (f) at shear rate of $2.422\tau_0^{-1}$. The volume fraction of system is 58%, and the mass fraction is 70%. The colloidal particles are all with diameter of $1.52\sigma_0$ and solvent particles are all with diameter of $0.05\sigma_0$ in this figure.

Table 1
Summary of the parameters in solutions with different particle diameter.

d	m	N	ε	σ_{cc}	σ_{cs}
σ_0	$1.79m_0$	100	ε_0	σ_0	$0.50\sigma_0$
$1.20\sigma_0$	$2.58m_0$	69	$1.20\varepsilon_0$	$1.20\ \sigma_0$	$0.60\sigma_0$
$1.36\sigma_0$	$3.31m_0$	54	$1.36\varepsilon_0$	$1.36\sigma_0$	$0.68\sigma_0$
$1.41\sigma_0$	$3.56\ m_0$	50	$1.41\ \varepsilon_0$	$1.41\ \sigma_0$	$0.705\sigma_0$
$1.52\sigma_0$	$4.14m_0$	43	$1.52\varepsilon_0$	$1.52\ \sigma_0$	$0.76\sigma_0$

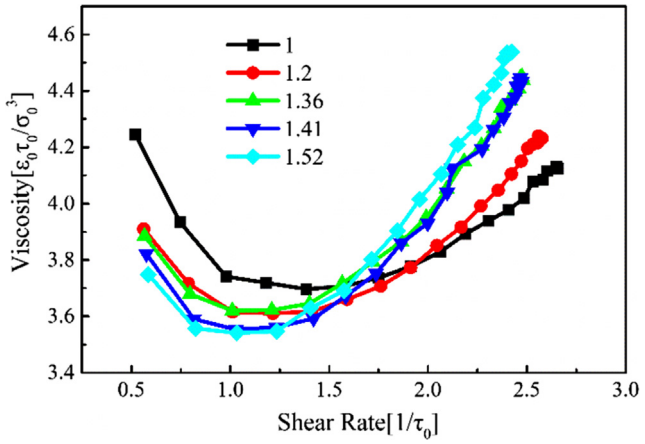

Fig. 4. Shear viscosity versus shear rate in suspensions with different particle diameters of σ_0, $1.2\sigma_0$, $1.36\sigma_0$, $1.41\sigma_0$, $1.52\sigma_0$. The other parameters are listed in Table 1.

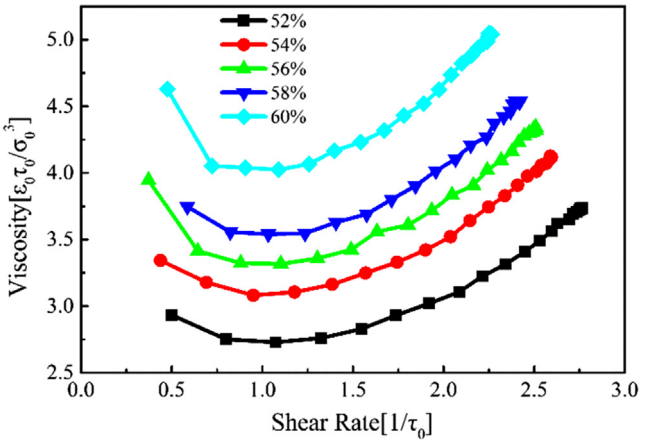

Fig. 6. Shear viscosity versus shear rate in suspensions with the volume fraction of colloidal particles varying by 52%, 54%, 56%, 58%, 60%. The colloidal particle diameter is $1.52\sigma_0$, number is 39, 41, 42, 43, 45, respectively, and other parameters are listed in Table 1.

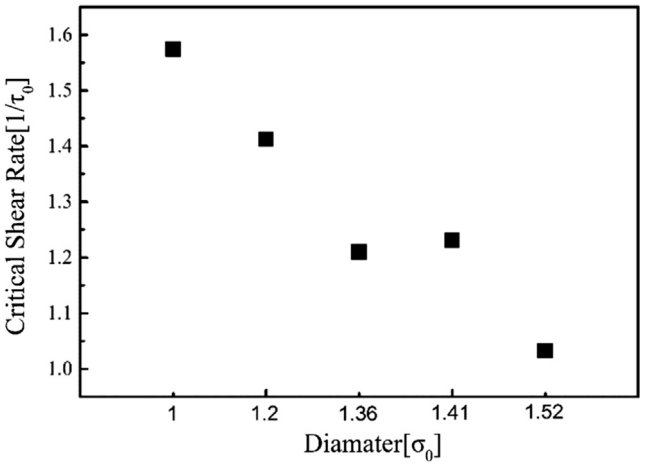

Fig. 5. Critical shear rate as function of colloidal particle diameter at volume fraction of 58%, mass fraction of 70%.

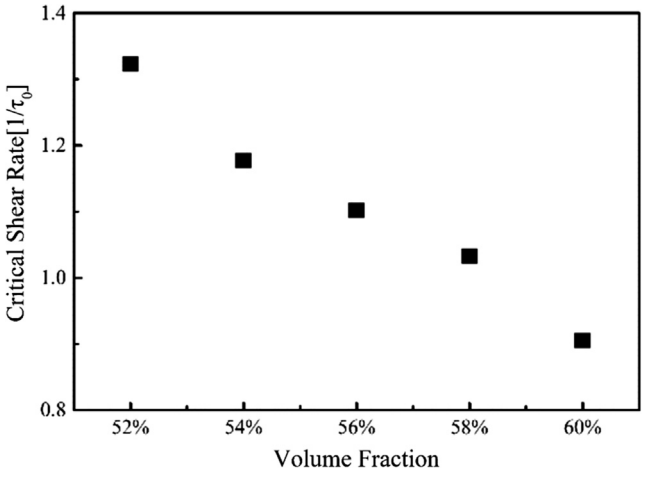

Fig. 7. Critical shear rate as function of volume fraction of colloidal particles, of which the diameter is $1.52\sigma_0$, and other corresponding parameters are listed in Table 1.

to the ST behavior. In addition, with the further increase of shear rate, the orientation of the string structure starts to deviate from the shear direction, which generates more resistance force on the flow with the deflection angle increasing. Therefore, the apparent viscosity of the whole system increases with the microstructure evolves from curve string to two-dimensional cluster.

3.2. Influences of diameter of colloidal particles

The volume fraction of colloidal particles is set as 58%, and the mass fraction is set as 70%. The diameter of colloidal particles is set as a variable to explore its influence on ST behavior. All parameters are shown in Table 1. As shown in Fig. 4, the larger the diameter of colloidal particles is, the lower the viscosity under low shear rate is. The original viscosity is 4.256 $\varepsilon_0\tau_0/\sigma_0^3$ at shear rate of 0.52 τ_0^{-1} for solution with particle diameter of σ_0, while that is $3.748\varepsilon_0\tau_0/\sigma_0^3$ at shear rate of $0.586\tau_0^{-1}$ for solution with particle diameter of $1.52\sigma_0$. However, the results are reversed at high shear rates. The maximum viscosity is $4.132\varepsilon_0\tau_0/\sigma_0^3$ at shear rate of $2.650\tau_0^{-1}$ for solution with particle diameter of σ_0, while that is $4.538\varepsilon_0\tau_0/\sigma_0^3$ at shear rate of $2.422\tau_0^{-1}$ for solution with particle diameter of $1.52\sigma_0$. Totally, the apparent viscosity first shows the shear-thinning behavior and then CST behavior with the increase of shear rate. Here we define the shear rate corresponding to the lowest apparent viscosity as the critical shear rate, at which the rheological behavior changes from shear-thinning to ST. And the

critical shear rate vs. particle diameter is plotted in Fig. 5. It shows that as the particle diameter increases, the critical shear rate decreases. In the simulation system, as the particle diameter increases, the increased attraction between particles induces that the layered structure can form in smaller shear rate. On the other hand, the increased repulsive force makes the layered structure more unstable, which leads to the earlier transition to ST under hydrodynamics action. Therefore, solution with bigger particle size can get into the ST state at smaller shear rate. Comparing with the experiment data in references [11,37], the tendency of critical shear rate vs. diameter in our simulation is credible.

3.3. Influences of volume fraction of colloidal particles

The volume fraction of colloidal particles is also taken into consideration to see if there is any influence on ST effects. In this period, the diameter of colloidal particles is set as $1.52\sigma_0$, the corresponding parameters are taken as listed in Table 1. The number of colloidal particles varies by 39, 41, 42, 43 and 45, to achieve the volume fraction of 52%, 54%, 56%, 58% and 60%, respectively. Generally, evident ST behaviors can be seen in all simulated solutions. The calculated viscosities are positively correlated with the volume fractions of colloidal particles over shear rates. In detail, at low volume fraction (i.e. 52%), the original viscosity is $2.934\varepsilon_0\tau_0/\sigma_0^3$, the minimum viscosity is $2.729\varepsilon_0\tau_0/\sigma_0^3$, and the maximum viscosity is $3.739\varepsilon_0\tau_0/\sigma_0^3$. At high volume fraction like 60%, the original viscosity is $4.631\varepsilon_0\tau_0/\sigma_0^3$, the minimum viscosity is $4.025\varepsilon_0\tau_0/\sigma_0^3$, and the maximum viscosity during ST stage is $5.042\varepsilon_0\tau_0/\sigma_0^3$. The degree of ST at volume fraction of 52% is far larger than that at volume fraction of 60%, which is defined as the maximum viscosity divided by the original viscosity. All is shown in Fig. 6. The critical shear rate vs. particle diameter is plotted in Fig. 7. It shows that as the volume fraction of colloidal particles increases, the critical shear rate decreases. With the increase of phase volume fraction, there is more collision probability between different particles. The number of synergistic pair should be increased and the layered structure can be formed at a smaller shear rate. Since the opportunity of collision between the particles in layered structure and other particles increases, the layered structure becomes even more unstable. It makes the whole system get into the ST state earlier. Thus, the critical shear rate reduces when the volume fraction increases within limits, as shown in Fig. 6. The influence of volume fraction on ST behavior in this work is consistent with both experimental and simulation data in references [31,53,54].

4. Conclusion

On the basis of the reported approaches [39–43], the hybrid SRD-MD mesoscale method with MP reverse perturbation algorithm is adopted to study the non-Newton rheological behaviors of STF. The evolution of microstructure of colloidal particles is firmly connected to the change of apparent viscosity under different shear rates in colloidal suspensions, consistent with results in previous literatures [32–35]. As the shear rate raises, the microstructure of colloidal particles changes to two-atom structures, layered structures, curve string structures, and finally two-dimensional clusters, corresponding to the viscosity first decreasing, then increasing, and finally reaching its maximum value. Under low shear rates, the hydrodynamic action is weak, which induces that two or three atoms in adjacent layers to be combined as a synergetic pair due to the attraction between particles. At higher shear rates, the synergetic pair structure extends because of the increasing hydrodynamics action, and transforms into a layered structure along flow direction. Since the layered structure has the lowest resistance to the local flow, the whole system shows the lowest apparent viscosity at that moment and can be regarded as a transition region, from which the apparent viscosity of the system changes from shear-thinning behavior to the ST behavior. Then, as the shear rate raises continuously, the layered structure is unstable. These layered structures rotate and collide with particles in adjacent layers to form a particle string. The orientation of these strings is random, and some of them are in a curve state. And with the orientation of the string structure deviating from the shear direction, more resistance acts on the flow, which results in continuous ST behavior occurring with shear rate increasing. At the highest shear rate, the strings curve more severely and get into two-dimensional cluster. This correspondence between microstructure and viscosity under shear in STF is consistent well with the mechanism of "hydro-cluster" [14–23]. The influence of particle diameter and volume fraction of colloidal particle on the evolution of colloidal particle microstructure during ST are also investigated from the perspective of mesoscale particle simulation in this work, which is in good agreement with the results in previous literatures [11,27,37,52–54]. This work can also guide the further work in laboratory experiments of preparing remarkable STFs. Closer correspondence between simulation and experiment and more impact factors in the field of colloid and interface science, like the temperature, surface modification and others, will be explored in our further work.

Acknowledgement

Financial supports from the National Natural Science Foundation of China (Grant No. 11372301), the fundamental research funds for the Central Universities (WK2480000002), and the Strategic Priority Research Program of the Chinese Academy of Sciences (Grant No. XDB22040502) are gratefully acknowledged. This work was also supported by Collaborative Innovation Center of Suzhou Nano Science and Technology.

Reference

[1] Y.S. Lee, E.D. Wetzel, N.J. Wagner, The ballistic impact characteristics of Kevlar® woven fabrics impregnated with a colloidal shear thickening fluid, J. Mater. Sci. 38 (2003) 2825–2833, http://dx.doi.org/10.1023/A:1024424200221.
[2] D. Zielinska, B. Delczyk-Olejniczak, L. Wierzbicki, B. ż ena Wilbik-Hałgas, M.H. Struszczyk, M. Leonowicz, Investigation of the effect of para-aramid fabric impregnation with shear thickening fluid on quasi-static stab resistance, Text. Res. J. 84 (2014) 1569–1577, http://dx.doi.org/10.1177/0040517514525881.
[3] A. Majumdar, B.S. Butola, A. Srivastava, Development of soft composite materials with improved impact resistance using Kevlar fabric and nano-silica based shear thickening fluid, Mater. Design. 54 (2013) 295–300, http://dx.doi.org/10.1016/j.matdes.2013.07.086.
[4] M. Hasanzadeh, V. Mottaghitalab, The role of shear-thickening fluids (STFs) in ballistic and stab-resistance improvement of flexible armor, J. Mater. Eng. Perform. 23 (2014) 1182–1196, http://dx.doi.org/10.1007/s11665-014-0870-6.
[5] M. Li, B. Lyu, J. Yuan, W. Yao, F. Zhou, M. Zhong, Evolution and equivalent control law of surface roughness in shear-thickening polishing, Int. J. Mach. Tool. Manu. 108 (2016) 113–126, http://dx.doi.org/10.1016/j.ijmachtools.2016.06.007.
[6] M. Li, B. Lyu, J. Yuan, C. Dong, W. Dai, Shear-thickening polishing method, Int. J. Mach. Tool. Manu. 94 (2015) 88–99, http://dx.doi.org/10.1016/j.ijmachtools.2015.04.010.
[7] C.D. Cwalina, C.M. McCutcheon, R.D. Dombrowski, N.J. Wagner, Engineering enhanced cut and puncture resistance into the thermal micrometeoroid garment (TMG) using shear thickening fluid (STF)–Armor™ absorber layers, Compos. Sci. Technol. 131 (2016) 61–66, http://dx.doi.org/10.1016/j.compscitech.2016.06.001.
[8] R.L. Hoffman, Discontinuous and dilatant viscosity behavior in concentrated suspensions. II. Theory and experimental tests, J. Colloid. Interf. Sci. 46 (3) (1974) 491–506, http://dx.doi.org/10.1016/0021-9797(74)90059-9.
[9] D.I. Dratler, W.R. Schowalter, R.L. Hoffman, Dynamic simulation of shear thickening in concentrated colloidal suspensions, J. Fluid. Mech. 353 (1997) 1–30, http://dx.doi.org/10.1017/S0022112097007167.
[10] J.W. Egmond, Shear-thickening in suspensions, associating polymers, worm-like micelles, and poor polymer solutions, Curr. Opin. Colloid. In. 3 (1998) 385–390, http://dx.doi.org/10.1016/S1359-0294(98)80054-X.

[11] R.L. Hoffman, Explanations for the cause of shear thickening in concentrated colloidal suspensions, J. Rheol. 42 (1998) 111–123, http://dx.doi.org/10.1122/1.550884.
[12] B.J. Maranzano, N.J. Wanger, Flow-small angle neutron scattering measurements of colloidal dispersion microstructure evolution through the shear thickening transition, J. Chem. Phys. 117 (2002) 10291–10302, http://dx.doi.org/10.1063/1.1519253.
[13] J.R. Melrose, R.C. Ball, Continuous shear thickening transitions in model concentrated colloids—the role of interparticle forces, J. Rheol. 48 (2004) 937–960, http://dx.doi.org/10.1122/1.1784783.
[14] B.J. Maranzano, N.J. Wagner, The effects of particle size on reversible shear thickening of concentrated colloidal dispersions, J. Chem. Phys. 114 (2001) 10514–10527, http://dx.doi.org/10.1063/1.1373687.
[15] V. Gopalakrishnan, C.F. Zukoski, Effect of attractions on shear thickening in dense suspensions, J. Rheol. 48 (2004) 1321–1344, http://dx.doi.org/10.1122/1.1784785.
[16] D.P. Kalman, N.J. Wagner, Microstructure of shear-thickening concentrated suspensions determined by flow-USANS, Rheol. Acta. 48 (2009) 897–908, http://dx.doi.org/10.1007/s00397-009-0351-2.
[17] C.D. Cwalina, N.J. Wagner, Rheology of non-Brownian particles suspended in concentrated colloidal dispersions at low particle Reynolds number, J. Rheol. 60 (1) (2016) 47–59, http://dx.doi.org/10.1122/1.4935445.
[18] C.D. Cwalina, N.J. Wagner, Material properties of the shear-thickened state in concentrated near hard-sphere colloidal dispersions, J. Rheol. 58 (2014) 949–967, http://dx.doi.org/10.1122/1.4876935.
[19] A.K. Gurnon, N.J. Wagner, Microstructure and rheology relationships for shear thickening colloidal dispersions, J. Fluid. Mech. 769 (2015) 242–276, http://dx.doi.org/10.1017/jfm.2015.128.
[20] S. Khandavalli, J.P. Rothstein, Large amplitude oscillatory shear rheology of three different shear-thickening particle dispersions, Rheol. Acta. 54 (2015) 601–618, http://dx.doi.org/10.1007/s00397-015-0855-x.
[21] J.F. Morris, A review of microstructure in concentrated suspensions and its implications for rheology and bulk flow, Rheol. Acta. 48 (8) (2009) 909–923, http://dx.doi.org/10.1007/s00397-009-0352-1.
[22] I.R. Peters, S. Majumdar, H.M. Jaeger, Direct observation of dynamic shear jamming in dense suspensions, Nature 532 (7598) (2016) 214–217, http://dx.doi.org/10.1038/nature17167.
[23] A.Y. Malkin, V.G. Kulichikhin, Shear thickening and dynamic glass transition of concentrated suspensions. State of the problem, Colloid. J. 78 (1) (2016) 1–8, http://dx.doi.org/10.1134/S1061933X16010105.
[24] J. Jerome, N. Vandenberghe, Y. Forterre, Unifying impacts in granular matter from quicksand to cornstarch, Phys. Rev. Lett. 117 (9) (2016) 098003, http://dx.doi.org/10.1103/PhysRevLett.117.098003.
[25] H.M. Laun, Rheological properties of aqueous polymer dispersions, Angew. Makromol. Chem. 123 (1) (1984) 335–359, http://dx.doi.org/10.1002/apmc.1984.051230115.
[26] A. Antosik, M. Głuszek, R. Żurowski, M. Szafran, Effect of SiO_2 particle size and length of poly (propylene glycol) chain on rheological properties of shear thickening fluids, Arch. Metall. Mater. 61 (3) (2016) 1511–1514, http://dx.doi.org/10.1515/amm-2016-0247.
[27] H.A. Barnes, Shear-thickening ("Dilatancy") in suspensions of nonaggregating solid particles dispersed in Newtonian liquids, J. Rheol. 33 (2) (1989) 329–366, http://dx.doi.org/10.1122/1.550017.
[28] B.J. Maranzano, N.J. Wagner, The effects of interparticle interactions and particle size on reversible shear thickening: hard-sphere colloidal dispersions, J. Rheol. 45 (5) (2001) 1205–1222, http://dx.doi.org/10.1122/1.1392295.
[29] A.D. Moriana, T. Tian, V. Sencadas, W. Li, Comparison of rheological behaviors with fumed silica-based shear thickening fluids, Korea-Aust. Rheol. J. 28 (3) (2016) 197–205, http://dx.doi.org/10.1007/s13367-016-0020-9.
[30] E. Brown, N.A. Forman, C.S. Orellana, H. Zhang, B.W. Maynor, D.E. Betts, Generality of shear thickening in dense suspensions, Nat. Mater. 9 (3) (2010) 220–224, http://dx.doi.org/10.1038/nmat2627.
[31] X.Z. Zhang, W.H. Li, X.L. Gong, The rheology of shear thickening fluid (STF) and the dynamic performance of an STF-filled damper, Smart. Mater. Struct. 17 (3) (2008) 035027, http://dx.doi.org/10.1088/0964-1726/17/3/035027.
[32] A.R. de Castro, M. Oostrom, N. Shokri, Effects of shear-thinning fluids on residual oil formation in microfluidic pore networks, J. Colloid. Interf. Sci. 472 (2016) 34–43, http://dx.doi.org/10.1016/j.jcis.2016.03.027.
[33] L. Gentile, B.F. Silva, S. Balog, K. Mortensen, U. Olsson, Structural transitions induced by shear flow and temperature variation in a nonionic surfactant/water system, J. Colloid. Interf. Sci. 372 (1) (2012) 32–39, http://dx.doi.org/10.1016/j.jcis.2012.01.027.
[34] N.N. Ling, A. Haber, E.O. Fridjonsson, E.F. May, M.L. Johns, Shear-induced emulsion droplet diffusion studies using NMR, J. Colloid. Interf. Sci. 464 (2016) 229–237, http://dx.doi.org/10.1016/j.jcis.2015.11.013.
[35] D. Spain, S. Troost, M. Golombok, Shear induced structure additives and nonlinear pressure drop effects in permeable flow, J. Colloid. Interf. Sci. 338 (1) (2009) 261–265, http://dx.doi.org/10.1016/j.jcis.2009.06.026.
[36] D.R. Foss, J.F. Brady, Structure, diffusion and rheology of Brownian suspensions by Stokesian dynamics simulation, J. Fluid. Mech. 407 (2000) 167–200, http://dx.doi.org/10.1017/S0022112099007557.
[37] N. Mai-Duy, N. Phan-Thien, B.C. Khoo, Investigation of particles size effects in dissipative particle dynamics (dpd) modelling of colloidal suspensions, Comput. Phys. Commu. 189 (2015) 37–46, http://dx.doi.org/10.1016/j.cpc.2014.12.003.
[38] M. Kroupa, M. Vonka, M. Soos, J. Kosek, Utilizing the discrete element method for the modeling of viscosity in concentrated suspensions, Langmuir 32 (33) (2016) 8451–8460, http://dx.doi.org/10.1021/acs.langmuir.6b02335.
[39] T. Ihle, D.M. Kroll, Stochastic rotation dynamics: a Galilean-invariant mesoscopic model for fluid flow, Phys. Rev. E. 63 (2) (2001) 020201, http://dx.doi.org/10.1103/PhysRevE.63.020201.
[40] G. Gompper, T. Ihle, D.M. Kroll, R.G. Winkler, Multi-particle collision dynamics: a particle-based mesoscale simulation approach to the hydrodynamics of complex fluids, Adv. Polym. Sci. 221 (2008) 1–87, http://dx.doi.org/10.1007/978-3-540-87706-6_1.
[41] W.C. Swope, H.C. Andersen, P.H. Berens, K.R. Wilson, A computer simulation method for the calculation of equilibrium constants for the formation of physical clusters of molecules: application to small water clusters, J. Chem. Phys. 76 (1) (1982) 637–649, http://dx.doi.org/10.1063/1.442716.
[42] F. Müller-Plathe, A simple nonequilibrium molecular dynamics method for calculating the thermal conductivity, J. Chem. Phys. 106 (14) (1997) 6082–6085, http://dx.doi.org/10.1063/1.473271.
[43] P. Bordat, F. Müller-Plathe, The shear viscosity of molecular fluids: A calculation by reverse nonequilibrium molecular dynamics, J. Chem. Phys. 116 (8) (2002) 3362–3369, http://dx.doi.org/10.1063/1.1436124.
[44] J. Castillo-Tejas, O. Castrejón-González, S. Carro, V. González-Coronel, J.F.J. Alvarado, O. Manero, Associative polymers. Part III: shear rheology from molecular dynamics, Colloid. Surfaces. A. 491 (2016) 37–49, http://dx.doi.org/10.1016/j.colsurfa.2015.11.052.
[45] H.A. Vinutha, S. Sastry, Disentangling the role of structure and friction in shear jamming, Nat. Phys. 12 (6) (2016) 578–583, http://dx.doi.org/10.1038/nphys3658.
[46] N.Y. Lin, C. Ness, M.E. Cates, J. Sun, I. Cohen, Tunable shear thickening in suspensions, P. Natl. Acad. Sci. USA 113 (39) (2016) 10774–10778, http://dx.doi.org/10.1073/pnas.1608348113.
[47] L.E. Silbert, J.R. Melrose, R.C. Ball, The rheology and microstructure of concentrated, aggregated colloids, J. Rheol. 43 (3) (1999) 673–700, http://dx.doi.org/10.1122/1.551028.
[48] S.B. Dan, G.S. Grest, J.B. Lechman, F. Pierce, S.J. Plimpton, P.R. Schunk, Particle dynamics modeling methods for colloid suspensions, Comp. Part. Mech. 1 (3) (2014) 321–356, http://dx.doi.org/10.1007/s40571-014-0007-6.
[49] M. Yamanoi, C. Leer, F.W.J. Van Hattum, O.S. Carneiro, J.M. Maia, Direct fibre simulation of carbon nanofibres suspensions in a Newtonian fluid under simple shear, J. Colloid. Interf. Sci. 347 (2) (2010) 183–191, http://dx.doi.org/10.1016/j.jcis.2010.03.069.
[50] X. Cheng, J. McCoy, J. Israelachvili, I. Cohen, Imaging the microscopic structure of shear thinning and thickening colloidal suspensions, Science 333 (6047) (2011) 1276–1279, http://dx.doi.org/10.1126/science.1207032.
[51] X. Cheng, X. Xu, S.A. Rice, S.R. Dinner, I. Cohen, Assembly of vorticity-aligned hard-sphere colloidal strings in a simple shear flow, P. Natl. Acad. Sci. USA 109 (1) (2012) 63–67, http://dx.doi.org/10.1073/pnas.1118197108.
[52] A.M.K. Laganapan, A. Videcoq, M. Bienia, T. Ala-Nissila, D. Bochicchio, R. Ferrando, Computation of shear viscosity of colloidal suspensions by SRD-MD, J. Chem. Phys. 142 (14) (2015) 144101-1–144101–8, http://dx.doi.org/10.1063/1.4917039.
[53] X.Z. Zhang, W.H. Li, X.L. Gong, Study on magnetorheological shear thickening fluid, Smart. Mater. Struct. 17 (1) (2008) 015051, http://dx.doi.org/10.1088/0964-1726/17/1/015051.
[54] N.C. Crawford, L.B. Popp, K.E. Johns, L.M. Caire, B.N. Peterson, M.W. Liberatore, Shear thickening of corn starch suspensions: does concentration matter?, J Colloid. Interf. Sci. 396 (6) (2013) 83–89, http://dx.doi.org/10.1016/j.jcis.2013.01.024.